Development and optimization of trivalent chromium electrodeposit on 304L stainless steel to improve corrosion resistance in chloride-containing environment

Okonkwo, Bright O.; Jeong, Chaewon; Lee, Hyeon Bae; Jang, Changheui; Rahimi, Ehsan; Davoodi, Ali

DOI
10.1016/j.heliyon.2023.e22538

Publication date
2023

Document Version
Final published version

Published in
Heliyon

Heliyon 9 (2023) e22538

Contents lists available at ScienceDirect

Heliyon

journal homepage: www.cell.com/heliyon

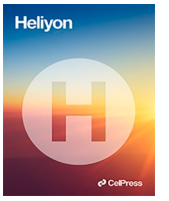

Development and optimization of trivalent chromium electrodeposit on 304L stainless steel to improve corrosion resistance in chloride-containing environment

Bright O. Okonkwo [a], Chaewon Jeong [a], Hyeon Bae Lee [a], Changheui Jang [a,*], Ehsan Rahimi [b], Ali Davoodi [c,d]

[a] Department of Nuclear and Quantum Engineering, Korea Advanced Institute of Science and Technology (KAIST), Daejeon, 34141, Republic of Korea
[b] Department of Materials Science and Engineering, Delft University of Technology, Mekelweg 2, 2628, CD, Delft, the Netherlands
[c] Materials and Metallurgical Engineering Department, Faculty of Engineering, Ferdowsi University of Mashhad, Mashhad, 9177948974, Iran
[d] Sichuan University-Pittsburgh Institute (SCUPI), Chengdu, 610207, China

ARTICLE INFO

Keywords:
Chromium
Electrodeposition
Coatings
Corrosion

ABSTRACT

In this study, we developed and optimized a trivalent chromium coating electrodeposited on 304L stainless steel (SS) from a Cr-trivalent bath. The results reveal that the Cr coatings at all bath temperatures except for 80 °C showed clusters of polyhedral grains, however, the grain sizes decreased with an increase in bath temperature. Also, the coatings deposited at bath temperatures of 30, 50, and 60 °C experienced networks of cracks, which decreased in population density as temperature increased. However, the coatings deposited at bath temperatures of 70 and 80 °C were crack-free due to surface modification, confirmed by 3D profile results with an advanced power spectral density and a multi-Gaussian histogram analysis. The mechanical test results demonstrate that the adhesion and wear resistance of the Cr-coatings formed on the SS substrate significantly improved, with the optimal coefficient of friction of 0.18. Likewise, electrochemical behavior observations of the Cr coatings show that pitting resistance improved with the increase in bath temperature conditions, as shown in the pitting potential values which increased from 272.6 mV to 436.2 mV as bath temperature increases from 30 °C to 80 °C. From this study, it is proposed that the Cr-coatings deposited at a bath temperature of 80 °C presents the optimal coating performance concerning a combination of all the target qualities aimed, such as better tribological behavior and improved pitting resistance. Thus, enabling the establishment of an innovative method to overcome the conventional issues encountered in Cr electrodeposition of SSs.

1. Introduction

Over the years, chromium (Cr) has frequently been utilized as a surface coating in various industrial applications such as general engineering products and automotive industry owing to its magnificent wear resistance, high resistance to heat and corrosion, and low coefficient of friction [1,2]. Based on these advantages, several coating methods have been developed to coat Cr on diverse surfaces,

* Corresponding author.
E-mail address: chjang@kaist.ac.kr (C. Jang).

https://doi.org/10.1016/j.heliyon.2023.e22538
Received 31 July 2023; Received in revised form 2 November 2023; Accepted 14 November 2023
Available online 19 November 2023

such as physical coating spray, plasma nitriding, electrodeposition, vapor deposition and others [3,4]. Among these methods, electrodeposition stands out because of its flexible and simple approach of producing Cr coatings under normal pressure and room temperature, with advantages of good homogeneity of coating thickness, low cost, and propensity to coat substrates of complex geometrical construct [4]. Other than these benefits listed, the electrodeposition process offers a feasible way to control the growth kinetics of coatings, that is, rapid and highly repeatable, and as well allows a process of simply obtaining large coating surfaces with different morphologies [5].

Despite these advantages, Cr coatings via electrodeposition have experienced some issues such as the existence of cracks, and poor adhesion [6]. The Cr coating is passive in several environmental conditions, but still, there could be an exposure of the substrate to corrosion due to the presence of cracks, especially when Cr-plated components are exposed to fluctuating mechanical or thermal loads [6]. Consequently, it is strongly desired for improvements to be made on the process and the properties of the Cr deposits since it is of interest in the years to come, as in this study for stainless steel (SS) material components.

Stainless steels (SS) have found wide practical applications in diverse industrial fields owing to their exclusive wear resistance, mechanical properties and corrosion resistance. More recently, their application interest has captured high-temperature industrial services, especially in gas turbine and jet propulsion engines, steam and nuclear power plants [7]. However, it is known that SSs, when sensitized and highly stressed are vulnerable to stress corrosion cracking (SCC), especially in chloride-induced environments [7,8]. Therefore, there is a rising demand to improve pitting corrosion resistance and reduce SCC susceptibility of SS material components in service. To achieve this, Cr electrodeposition, amongst other methods, is perceived to be a cost-effective and easy technique [7], provided that the binding force between the coating and substrate is good.

Although, Cr electrodeposition may stand a chance of improving the SCC resistance of SS in chloride-induced environments, it is generally known that there exist some difficulties such as, poor adhesion of Cr electrodeposits on SS surfaces, owing to the quick formation of oxide film on its surfaces [7]. Also, Khani H. et al. [9] stated that in a Cr bath solution, a high overpotential is needed to reduce the electrochemically stable Cr-complex ions ($Cr(H_2O)_6)^{3+}$). This eventually leads to undesired hydrogen evolution reaction (HER) at the substrate of interest, resulting in poor coating properties and adhesion, and low current efficiency [9,10]. This problem is even more challenging when SS substrates are subject to Cr electrodeposition since they are known to have high electrocatalytic activity for the HER due to the presence of transition metals [11,12]. To resolve this issue, researchers proposed the use of nickel strike over the SS surface before Cr plating. However, this attempt has shown to be erratic in industrial applications [13], because the nickel strike procedure which produces more hydrogen gas than its deposit metal raises the risk of hydrogen embrittlement, and potential cracks in the deposited metal [14]. Thus, the need to further improve on the electrodeposition process to resolve the difficulties encountered in depositing Cr on SS is deemed important and necessitated this study.

In this study, the direct Cr plating of 304L SS storage canister is aimed. The SS storage canisters are used to temporarily store the spent nuclear fuel [8]. This spent nuclear fuel emits decay heat during storage period, which creates natural convection around the storage canisters, thereby causing outside air to cloud around the canister surface. With the passage of time, the decay heat drops and the storage canister cools, then water can condense on the canister surface and brine can form, which may cause pitting. The formation of the pit is seen as a precursor to chloride-induced stress corrosion cracking (CISCC). To provide letter protection to pitting and CISCC during the long-term storage of spent nuclear fuel, the application of Cr on susceptible locations of the canister is being considered. For that purpose, eco-friendly Cr coating on SS is targeted and investigated. Scanning electron microscope (SEM), X-ray diffraction (XRD), and 3D profilometry are utilized in characterizing the microstructure morphology and chemical composition, crystallinity, and surface topography distribution of the coatings, respectively. Mechanical test methods such as Vickers hardness test and scratch test are also employed in studying the mechanical behavior of the coatings concerning the different process conditions. Additionally, the surface wettability and electrochemical response of the Cr coatings are studied with a contact angle tester, and potentiodynamic polarization test, respectively. Detailed analysis of the 3D profilometry data, using histogram generated by multimodal Gaussian distribution fit and power spectra density (PSD) analysis [15,16], enabled prediction of localized corrosion damage and in-depth quantification. Our results will provide new insight into the role of electrodeposition operation temperature, microstructure, and surface topography of Cr coatings in both electrochemical activity and SCC resistance performance.

2. Experimental methods

2.1. Electrodeposition procedure and parameters of Cr coatings

2.1.1. Pre-treatment

In this study, a new pretreatment method was developed to enhance the coatings adhesion to the SS substrates when electroplated without a nickel strike layer. Also, the aim of the new method is to eliminate the erratic situations, such as red-rust associated with using nickel strike on SS substrate before Cr electroplating. By the new method, the ready to coat samples were cleaned in an alkaline cleaning bath containing 15 g/L NaOH, 25 g/L Na_2CO_3, and 25 g/L $Na_3PO_4.12H_2O$, at a bath temperature of 70 °C for 7 min. Thereafter, the samples were anodically electro-cleaned with the same solution at a current density of 2.14 A/dm^2 and cleaned with distilled water. Subsequently, anodic activation was applied to the air-formed oxide layer on the 304L SS after cleaning and before electroplating. The anodic activation was carried out by connecting the 304L SS as the anode in the electrolytic sulfuric acid (500 ml/L) bath circuit, with nickel as the cathode and at a current density and exposure time of 2.14 A/dm^2 and 1–1.5 min, respectively. Thereafter, the sulfuric acid is rinsed away, and the Cr deposit is applied immediately in a conventional manner. It is noticed that by using this method of reversing the flow of electrons away from the SS rather than to the SS, there is a remarkable improvement in the adherence of the Cr coating to the SS substrate as shown in the Supplementary Fig. S1. This adherence is unpredicted and contrary to

the typical understanding of the art that the part under electrolytic acid exposure should be cathodic in the electrical system. Also, Fig. S1c shows an image of the SS surface after anodic activation, which depicted a surface that was not attacked with pitting.

Prior to the electrodeposition, each working cathode (with dimension of 15 × 15 × 3 mm) was ground successively by 600, 1200, 2000, 4000, and 7000 grit of SiC abrasive papers to remove scratches. It is important to point out that absolute care was taken during sample preparation to eliminate sharp edges because of the vital role geometry of objects plays in how they receive electroplating. Literature [14] has reported that certain geometrical shapes (e.g. sharp edges) will result in more attraction of cations than other areas, and as such, the current density increases at that point and builds up much deposition. This results in brittle coating layer deposition that easily breaks off and becomes detrimental to the coated sample. After polishing, the prepared samples were ultrasonically cleaned in acetone for 3 h, and thereafter cleaned in distilled water.

2.1.2. Electrodeposition

Cr coatings were electrodeposited on 304L stainless steel samples from a chromium-sulfate electrolyte bath. The bath composition is listed in Table 1. The chemicals were added in the following order $Cr_2(SO_4)_3.6H_2O \rightarrow CO(NH_2)_2 \rightarrow Al_2(SO_4)_3.18H_2O \rightarrow Na_2SO_4 \rightarrow H_3BO_3 \rightarrow HCOOH \rightarrow C_{12}H_{25}NaSO_4$. The temperature of the bath during preparation was kept at 60 °C to increase the rate of reactions.

A two-electrode direct current system was used to electrodeposit the Cr coatings, with the 304L SS substrate as the working electrode (cathode) and a nickel plate as an anode. The electrodes distance was 3 cm. Different bath temperatures were employed, which are 30 °C, 50 °C, 60 °C, 70 °C, and 80 °C to determine the best condition. The current density and deposition duration for all bath temperature conditions were kept constant at 25 A/dm^2 and 1 h, respectively. The pH of the bath composition is 1.9. The electrodeposition was carried out within 2 min after anodic activation to ensure that the passive film was not reformed before electrodeposition.

2.2. Coating characterization

Scanning electron microscope (SEM, Hitachi SU5000) equipped with energy dispersive X-ray spectrometry (EDS), and X-ray diffractometer (Xiper, MPD, Philip) analyzer with CuKα radiation in the range of 10° – 90° and at a scan rate of 0.02°/s were used to characterize coating layers, such as morphology, composition, and structure of the coatings, respectively. The surface topography of the electrodeposited coatings before and after the electrochemical test was obtained with a 3D profilometer (Bruker Contour GT) and analyzed with vision 64 software. Advanced analysis was performed on the 3D profile images (before and after exposure to a corrosive environment) using a combination of Gaussian multimodal histogram and power spectra density (PSD) with the methodology used in previous studies [15,16]. The surface wettability of the bare 304L SS and coated 304L SS were examined by measuring the static contact angle (θ) at atmospheric pressure and room temperature using contact angle Phoenix MT(T) equipment and analyzed with TS view software. The contact angles were obtained at two locations on each sample to ensure the repeatability of results.

2.3. Mechanical property measurements

2.3.1. Microhardness

The microhardness of the Cr-coated samples and the bare 304L SS was measured by Vicker hardness indenter (Wolpert Wilson Instrument, model 402MVD). The dwelling time of analysis was 10 s with a load of 100 g. The average hardness value was obtained from five different locations of each sample.

2.3.2. Scratch test

Scratch test was employed to investigate the frictional behavior and damage to the Cr coating layers under sliding condition. A scratch tester from Ducom Instrument PVT LTD equipped with a Rockwell C-diamond stylus was used. Progressive load mode was employed to obtain the critical load at which failure occurred along the scratch track by applying a load from 0 to 10 N for a length of 5 mm. The equipment was furnished with an acoustic emission investigation system to identify crack formation and a framework to measure the horizontal frictional force (FF, F_t) in the scratching direction from which the coefficient of friction (COF) can be obtained ($F_t = \mu F_n$). The average values of COF and FF were calculated from the obtained COF and FF respective plot data. The extensive scratch test parameters are given in Table 2.

Table 1
Chemical composition of the electrolyte bath used for Cr electrodeposition.

Compounds	Amount (g/L)	Roles
$Cr_2(SO_4)_3.6H_2O$	235	Cr source
$CO(NH_2)_2$	30.03	Complexing agent
$Al_2(SO_4)_3.18H_2O$	99.96	Conducting salt
Na_2SO_4	42.61	Conducting salt
HCOOH	20	Complexing agent
H_3BO_3	30.91	Buffering agent
$C_{12}H_{25}NaSO_4$	0.08	Surfactant

Table 2
Experimental parameters for the scratch test on the Cr-coated materials.

Parameters	Values
Progressive load	0–10 N
Incremental load rate	2 μ/mm
Scratch speed	0.1 mm/s
Indenter tip material	Diamond
Tip radius	200 μm

2.4. Corrosion property measurement

The corrosion resistance of the electrodeposits was examined by using a potentiodynamic polarization test performed in a conventional three-electrode cell (Gamry 600 Instrument), with a saturated calomel electrode (SCE) as reference electrode, electrodeposited samples as a working electrode, and a platinum wire as a counter electrode. The tests were carried out in a 3.5 wt% NaCl environment at an ambient temperature of 25 ± 3 °C. During the potentiodynamic polarization test, the sweep potential range was from OCP to 0.5 V_{SCE} at a scanning rate of 5 mV/s, after OCP was obtained for 300 s. The pitting potential value was derived from the point of deflection of the current density, that is, the point where there was a sharp change in slope at the anodic arm of the curve. Duplicate tests were performed in each coating condition to enable repeatability of results.

3. Results and discussion

3.1. Microstructural and surface topography characterization of various coatings

Fig. 1a–(e) shows a series of SEM micrographs of the Cr-coatings deposited in the trivalent Cr bath at temperature conditions of 30 °C, 50 °C, 60 °C, 70 °C and 80 °C. Networks of cracks which decreased with increase in bath temperature are observed in the deposits formed at bath temperatures of 30 °C, 50 °C, and 60 °C, as seen in Fig. 1a(i) – c(i), respectively. In contrast, such networks of cracks are absent in the Cr layers deposited at 70 °C and 80 °C, as evident in Fig. 1d(i) and e(i) as well as the lower magnification images (Supplementary Fig. S2), although, some few cracks/pores which did not connect or form network were observed. Among the high temperature bath deposited coatings, the coatings deposited at 70 °C showed evidence of pores/pinholes, as depicted in the plane view and cross-section micrographs in Fig. 1d(i) and d(ii). The pores formed at this bath temperature condition may be as a result of hydrogen discharge, as reported in previous study [17]. To further investigate the coating defects and thickness, the cross-sections of the Cr coatings were analyzed and presented in Fig. 1a(ii) – e(ii). Crack penetration ability through the coating deposits decreased with increase in temperature of the bath, as shown in Fig. 1a(ii) – c(ii). The highly reduced crack formation or crack network formation noticed at 70 °C and 80 °C indicates that Cr deposition from a trivalent bath at a high temperature of 70 °C and above can effectively reduce the formation of cracks in the deposit.

Generally, the crack formation in Cr coating can be explained by the crystallization mechanism of the electrodeposited Cr. According to the literature [3,17,18], the electrodeposition of Cr from a trivalent Cr-bath is commonly linked with low current efficiency, which goes along with a substantially high level of hydrogen evolution. Subsequently, the reduced hydrogen is incorporated into the Cr coatings, and thus, results in the formation of metastable hexagonal chromium hydride (β-Cr). Afterwards, the β-Cr breaks down to form stable body-centered cubic (BCC) chromium (α-Cr) containing a residue of dissolved hydrogen and hydrogen gas. This decomposition occurs during the electrodeposition process and causes tensile stress, which invariably results in crack formation cracks in the coating.

The hydrogen in-corporation plays a pivotal role in the formation of crack in Cr coatings via two ways; First is the inducement of compressive stress coming from the retention of the incorporated hydrogen in the deposit, and secondly, the release of the incorporated hydrogen from the deposit can lead to the inducement of tensile stress [17]. However, at higher temperatures (70 °C and above), β-Cr formation and subsequent transformation, is too unstable to be produced during the plating process at high-temperature, and thus cracks induced by residual stress is not formed. Hence, crack-free α-Cr is readily deposited directly via hot chromium process, as has been obtained in this study and others [2].

Furthermore, from Fig. 1a(ii) – e(ii), it is clearly evident that the thickness of the Cr coating layer decreases with an increase in electrolyte bath temperature and that the coatings are homogenously and compactly attached to the SS substrate, thereby giving credence to the new pretreatment method employed in this study. The reason for the decrease in coating thickness with bath temperature increase may be related to the increased close competition of the first reduction step of Cr^{3+} to Cr^{2+} in Cr electrodeposition (−0.74 E°) and the reduction of water into hydrogen (−0.83 E°), of which their respective standard reduction potentials suggest. It has been reported previously that the reduction of water diminishes the cathode efficiency of Cr deposition [19]. Based on this, the current efficiency of the Cr-coatings plated at different bath conditions were calculated using Faraday's law of electrolysis [1,20] given in equation (1):

$$\Phi = \frac{w \times z \times F}{m \times q} \tag{1}$$

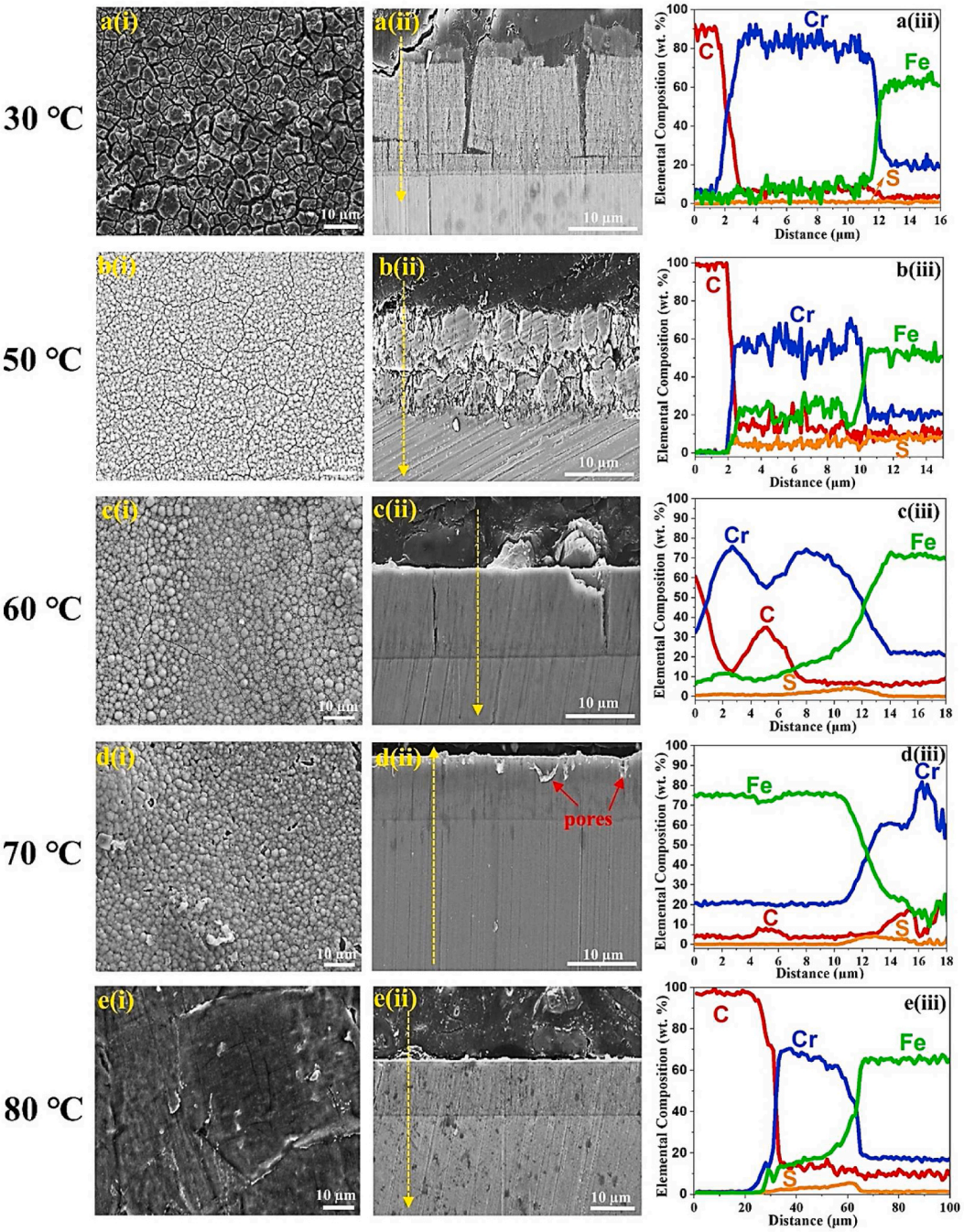

Fig. 1. SEM micrographs of the plane and cross-sectional views along with corresponding elemental line profiles of Cr-coated 304L SS for bath temperatures of (a) 30 °C, (b) 50 °C, (c) 60 °C, (d) 70 °C, and (e) 80 °C.

Table 3
Calculated current efficiency of Cr-coatings obtained at different bath temperatures.

Temperature (°C)	Current efficiency (%)	Average coating thickness (µm)
30	36	11.1
50	30	10.8
60	27	9.8
70	25	5.9
80	14	4.2

where w is the weight of the deposit (obtained by subtracting the initial weight of the 304L SS from its final weight after electrodeposition), z is electron stoichiometry ($3e^-$), F is Faraday's constant (96500 C/mol), m is the molar mass of Cr (51.97 g/mol), and q is the electrical charge (c is equal to I × t, and t and I are 60 s and 0.42 A, respectively).

The calculated current efficiency and average thickness of Cr coatings listed in Table 3 shows a decrease with respect to bath temperature increase, as noticed in previous study [18]. Notwithstanding, the calculated current efficiency values of this study are greater than that of other Cr trivalent bath, which is normally in the range of 10–25 % [17]. Such improvement may be due to the proper adhesion, as confirmed by the SEM image in Supplementary Fig. S1, and the inclusion of sodium dodecyl sulfate ($C_{12}H_{25}NaSO_4$) surfactant, which helped in decreasing the polarization of the cathode by adsorbing the SH-containing molecules, and in turn, induced the electrochemical discharge reaction by preventing hydrogen adsorption [19].

Comparing the morphologies, it is observed that the Cr coatings at all bath temperatures, except at 80 °C showed clusters of polyhedral grains. Also, the SEM images in Fig. 1a–(e) indicate that the increase in electrolyte bath temperature leads to surface modification, with coatings produced at higher temperatures showing smoother surfaces and decreasing size in the polyhedral granules. According to the literature, this phenomenon occurs owing to enhanced mass transport at higher bath temperatures [21]. This was further corroborated by the 3D topography profile images and extracted average roughness values (R_a) obtained from the Cr-coated specimens at different bath temperatures, as shown in Fig. 2.

From the topography maps of the electrodeposited Cr coatings at low temperatures of 30 °C (Figs. 2a) and 50 °C (Fig. 2b), we can observe the presence of various surface features with a heterogeneous distribution and a high surface roughness that directly correlated to the non-uniform surface cracks and large polyhedral granules, that is proved in SEM images. While from Fig. 2c-e it is observed that the coating surface roughness and value decreased with increase in bath temperature. To better visualize the surface features and roughness distribution in all electrodeposited Cr coatings, we conducted the histogram topography analysis using the topography maps in Fig. 2. According to the histogram analysis in Fig. 3a, Cr-coated surfaces deposited at both 30 °C and 50 °C exhibit a heterogeneous distribution of surface roughness with various peak intensities alongside the shifting of overall histogram peaks to higher roughness (height in the x-axis) in comparing to Cr-coated surfaces deposited at 60 °C, 70 °C and 80 °C. Although, only a single histogram peak with high intensity and very low roughness (overall histogram shifted to lowest roughness) was observed in Cr-coated surfaces deposited at 60 °C, 70 °C, and 80 °C. This surface analysis further can be validated by the extracted mean value and standard deviation of surface roughness (Fig. 3b). From this figure, Cr-coated surfaces deposited at 60 °C, 70 °C, and 80 °C in comparison to those at 30 °C and 50 °C represent the lowest mean value and standard deviation of surface roughness, which indicates better surface homogeneity and/or similarity of surface features.

The chemical composition of the electrodeposited Cr coating on the 304L SS at different bath temperature conditions was analyzed with SEM-EDS line scan (shown in Fig. 1a(ii) – e(ii)), and the results are presented in Fig. 1a(iii) – e(iii). From these elemental line profiles, it is evident that Cr, C, and S elements are present in the coatings deposited at all bath temperature conditions, which suggests that there is complex chromium compounds in the deposit. However, the percentage of C and S varied with temperature change, as shown in Fig. 4.

According to previous researches [22–24], the carbon co-deposited with Cr originates from the organic complexants like formic acid and urea, which are present in the electrolyte bath used. This occurs as a result of the electro-reduction of the organic substances during electroplating. While, the S co-deposition with Cr in the deposits originates from the surfactant present in the electrolyte bath. Authors have also reported that the deposition of C alongside of Cr frequently results in crack formation in the deposits, and consequently deteriorates the properties of the deposit. Interestingly, it is observed in this study that the amount of C diminishes greatly with

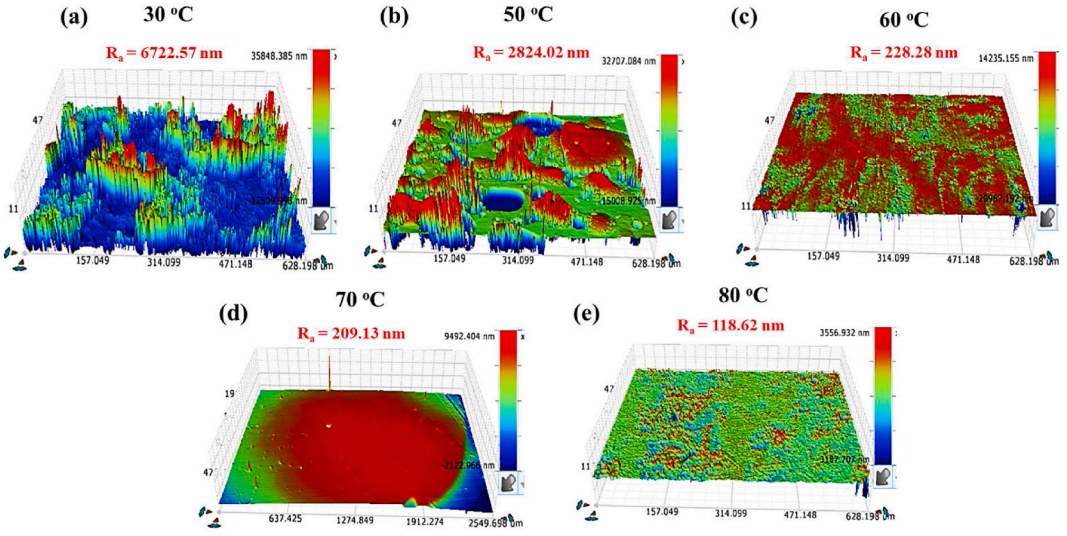

Fig. 2. 3D topography profile maps of Cr-coated 304L SS surfaces at bath temperatures of (a) 30 °C, (b) 50 °C, (c) 60 °C, (d) 70 °C, and (e) 80 °C.

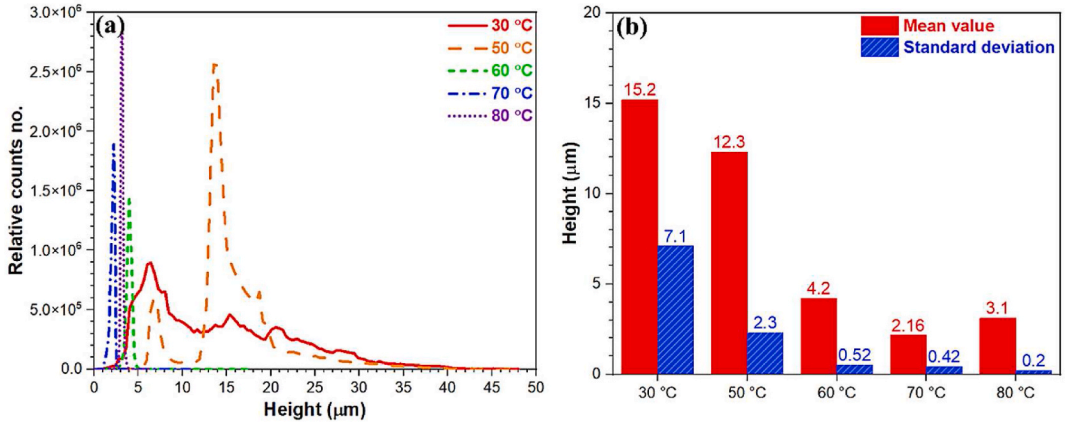

Fig. 3. (a) The multi-modal Gaussian histograms of surface roughness distribution of electrodeposited Cr coatings in Fig. 2 and (b) mean value and standard deviation calculations extracted from (a).

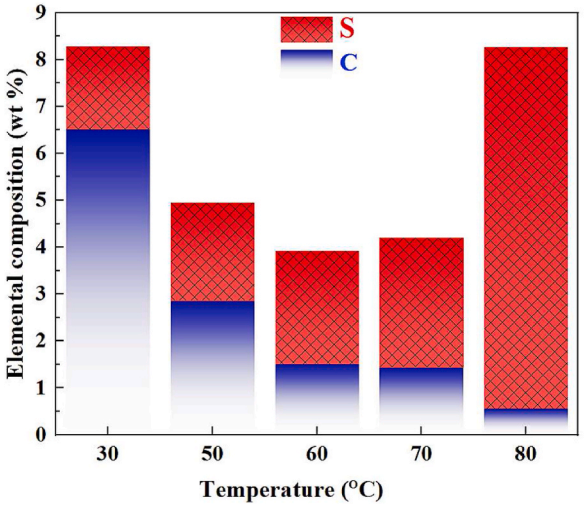

Fig. 4. SEM-EDS point scan results containing the elemental composition of C and S in the Cr electrodeposits plated at different bath temperature conditions.

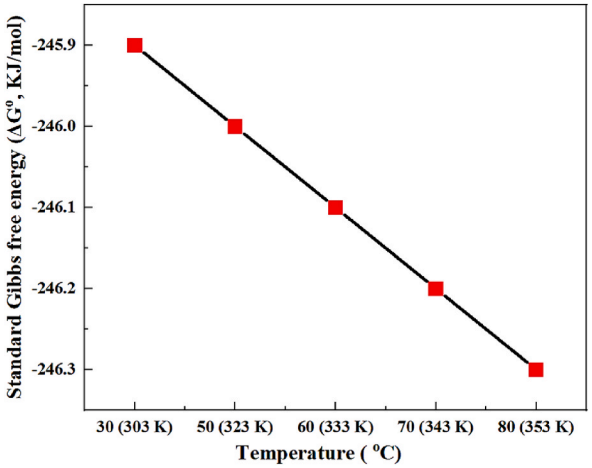

Fig. 5. Standard Gibbs free energy of CrS bond formation vs. temperature plot.

an increase in electrolyte bath temperature from 30 °C (C, 6.51 wt%) to 80 °C (C, 0.56 wt%). On the other hand, the content of S markedly increased as the electrolyte bath temperature increased from 30 °C (S, 1.77 wt%) to 80 °C (S, 7.71 wt%). This suggests that the substitution of C with S in the bond formation with Cr in the electrodeposit increases with bath temperature increase and possibly led to decreased crack density observed. To investigate this trend further, the standard Gibbs free energy of Cr–S bond formation in the temperature range studied was calculated with the formula in equation (2), of which part of the data used was obtained from the widely available compilation of standard state thermodynamics [25,26] and the chemical reaction in equation (3):

$$\Delta G = \Delta H^0 + T\Delta S^0 \tag{2}$$

$$Cr_{(aq)} + S_{(aq)} \rightarrow CrS_{(s)} \tag{3}$$

where ΔH^0 is the change in standard enthalpy (i.e product ($CrS_{(s)}$, −176 kJ/mol)) minus reactants ($Cr_{(aq)}$, 26.07 kJ/mol + $S_{(aq)}$, 41.8 kJ/mol)), T is the bath temperature (K) and ΔS^0 is the change in standard entropy (i.e product ($CrS_{(s)}$, 65 J/mol.K) minus reactants ($Cr_{(aq)}$, 36.20 J/mol.K + $S_{(aq)}$, 22 J/mol.K)).

The standard Gibbs free energies of Cr–S bond formation calculated from the standard values of entropy and enthalpy at various phases present in the reaction and at different bath temperatures show that the increase in temperature pushes the Gibbs free energy to a more negative value (as shown in Fig. 5), which increases the chances of spontaneity in the bond formation between Cr and S without any external force.

3.2. XRD and water contact angle analysis

To identify the structure of the deposited coatings, XRD experiment were performed on the Cr coated samples, and the findings are presented in Fig. 6. As demonstrated in Fig. 6, the characteristic peaks of Cr at 44°, 65°, 76°, and 82° attributed to (110), (200), (320) and (211) planes [27–30], respectively, were detected from the deposited Cr coatings at all bath temperatures.

Moreover, Fig. 6 shows that the Cr coating amorphization increases with decline in bath temperature, as evidenced by the broadening of the standard Cr peak at 44° for the Cr (110) plane. The increase in the degree of amorphization with a decrease in bath temperature is ascribed to the increased incorporation of metalloid carbon atoms in the chromium crystal lattice, which perturbs the setting order of the chromium atom [9,17,23,28,30]. This phenomenon is corroborated by the presence of chromium carbides (Cr_7C_3 and $Cr_{23}C_6$) peaks alongside with Cr peaks identified at peak angles indicated with the red lines in Fig. 6 [22,31], which decreased in intensity with temperature increase. The occurrence of increasing chromium carbide peaks and increasing amorphization with temperature bath decrease indicates C content increase in the Cr coating as bath temperature decreases, which is in accordance with the SEM-EDS result (Fig. 4). From the XRD pattern of the bare SS, it is seen that the sharp peak at 43.5° represents the bare metal, which contains much of Cr element as detected by the XRD peak, as well.

Additionally, it is noticed that chromium dioxide (CrO_2) peaks at 44.9°, 65°, and 82° (indicated with blue lines) [32–34] are detected in the Cr coatings deposited at all bath temperatures, except for 80 °C and with decreased intensity for 70 °C. The presence of

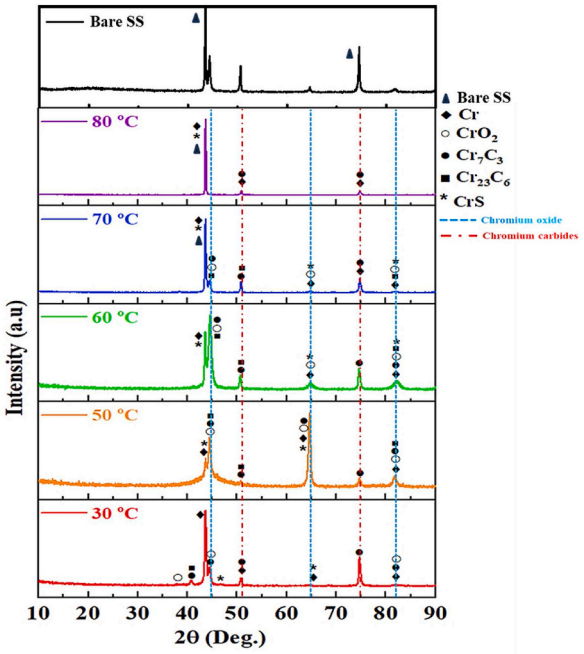

Fig. 6. XRD patterns of the electrodeposited Cr coatings at different bath temperatures from a chromium-sulfate trivalent Cr bath.

oxygen in the Cr coating is ascribed to two reasons depending on the reaction conditions: Firstly, it is due to the presence of hydroxide anions emanating from the competitive reduction of water in the trivalent Cr electrodeposition process, which is commonly linked with the reduction of the deposit thickness, as described earlier [19]. And secondly, the oxygen present in the Cr coating can originate from the adsorption of the Cr complexed species ($Cr(H_2O)_6)^{3+}$) that is not decomplexed at low temperatures [19]. Also, it is observed that the peaks of chromium sulfide (CrS) were present in the Cr coated samples, which agrees with the SEM-EDS analysis for S content and Gibbs free energy calculation for the degree of spontaneity of S in the electrodeposition reactions. The presence of S in the deposited coating arises from the sulfur-containing additive included in the bath. Chien et al. [17] demonstrated that sulfur-containing additives or presence in an electroplating trivalent Cr bath can remarkably enhance the crystallinity of the Cr–C deposit obtained from such bath.

Fig. 7 shows the water contact angle for uncoated 304L SS and Cr-coated 304L SS samples. The contact angle values inserted in the images (Fig. 7b–f) show that the Cr-coated samples all passed the hydrophobic mark ($> 90°$), while the contact angle of the uncoated SS (Fig. 7a) was below the hydrophobic mark or hydrophilic in nature ($<90°$). Thus, the result indicates that the surface wettability resistance of the 304L SS could be potentially enhanced by Cr electrodeposition, which in turn could be advantageous in the corrosion resistance of the material. Moreover, from Fig. 7, it can be seen that the hydrophobicity of the Cr coatings slightly increased with a decrease in bath temperature, which can be correlated with the surface roughness described in the SEM and 3D topography profile results. Conventionally, a rougher surface is more hydrophobic than a smother one [35,36], therefore, the Cr coatings with rougher surface should have the highest hydrophobicity, as in the case of the electrodeposited Cr coating at 30 °C in this study. The increasing sulfur content as against the carbon content with respect to bath temperature increase is another reason for the slight decrease in hydrophobicity of the Cr coatings deposited at higher temperatures, since sulfur is more electronegative than carbon, and as such has a higher affinity for water [36].

3.3. Mechanical behavior of the Cr coatings

Fig. 8 presents the hardness data for the bare 304L SS and Cr-coated 304L SS. The plot in Fig. 8 shows that the hardness decreases as the bath temperature increases.

The suggested reason for this behavior is that, as shown in Fig. 6, the chromium oxide and the chromium carbide at 44.5° and 64.5°, respectively, decreased as temperature increased, and as such, a decrease in the hardness values. Previously, authors have related the increase in hardness and internal stress leading to cracking to the presence or increase of chromium oxide and chromium carbides in the Cr coating [3]. In comparison, the hardness value for the bare stainless steel showed an improvement when Cr was electrodeposited at all bath temperature conditions, as indicated by the red arrow. This improvement could be advantageous in the SCC resistance of the applied Cr coatings, as will be investigated later in this study. However, it is important to point out that the substrate may have had little effect on the measured hardness of the coated samples, especially those deposited at high temperature bath, which has lower coating thickness as reported in section 3.1.

The coefficient of friction (COF) plot for all bath temperature conditions in Fig. 9a shows a downward trend with an increase in temperature, as also confirmed by their average values in Table 4. However, it is important to point out that the coefficient of friction trend of coating deposited at a bath temperature of 70 °C was slightly lower than that at a bath temperature of 80 °C, as shown in Fig. 9a. The downward trend in coefficient of friction with an increase in temperature signifies a better adhesion and improved wear resistance of the electrodeposited Cr coating to the 304L SS substrate [37]. Overall, Cr coating deposited at a bath temperature of 70 °C showed the best coating adhesion from the plot and average value in Fig. 9 and Table 4, respectively. Conversely, the COF curve of the Cr coating electrodeposited at a bath temperature of 30 °C exhibited the highest values and fluctuations, followed by that deposited at 50 °C. The high COF fluctuation at lower temperatures of 30 °C and 50 °C signifies the brittle nature of the coatings [37], which

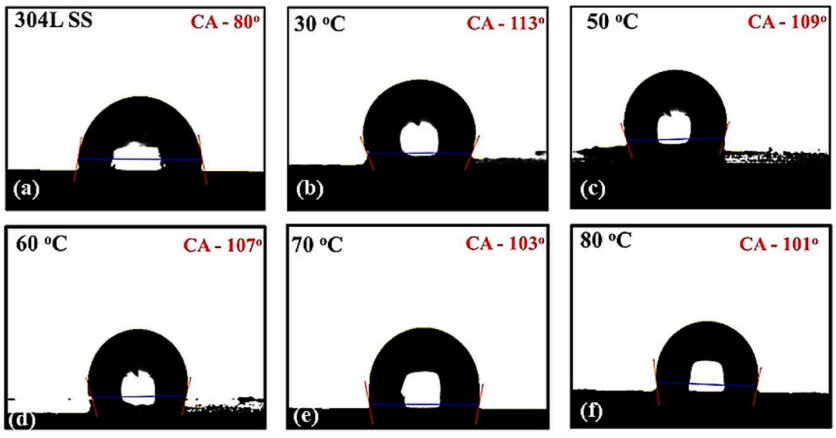

Fig. 7. Images of the water droplet on the uncoated 304L SS (a) and Cr-coated 304L SS samples (b–f) at all bath temperature conditions, with the average contact angle values inserted in each image.

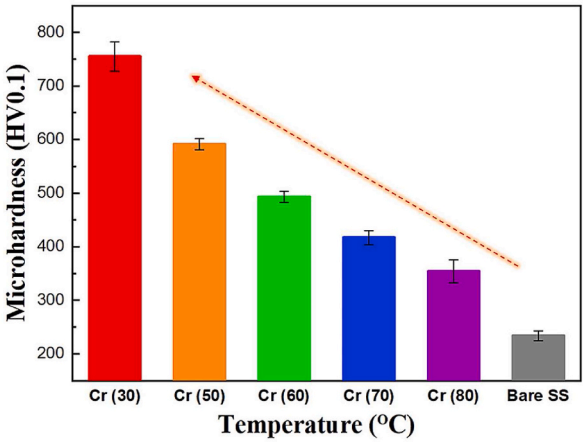

Fig. 8. Vickers hardness ($HV_{0.1}$) plot of the bare 304L SS and Cr-coated 304L SS samples at all bath temperature conditions.

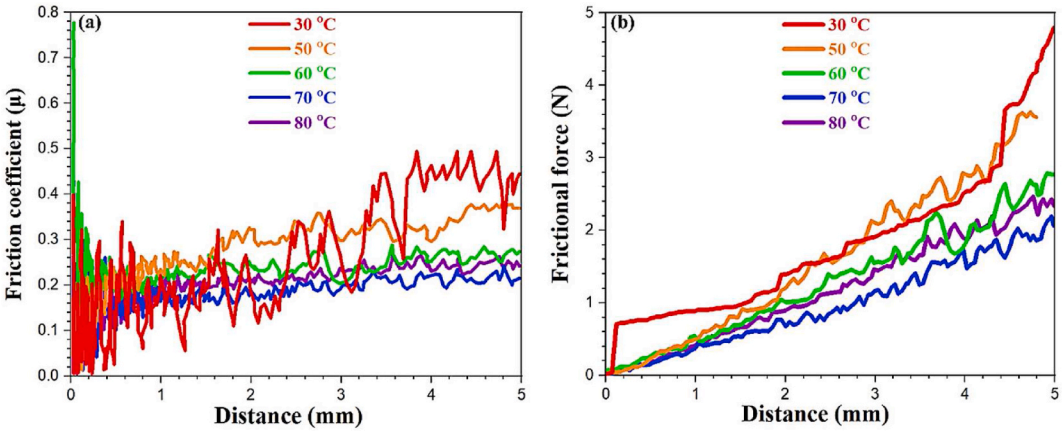

Fig. 9. (a) A plot of the coefficient of friction trend over a specific distance in the Cr-coated 304L SS samples, and (b) a plot of the frictional force trend over a specific distance in the Cr coated 304L SS samples at all bath temperature conditions studied.

Table 4
The average values of frictional force and coefficient of friction extrapolated from the plots in Fig. 9.

Temperature (°C)	FF (Avg.)	COF (Avg)
80 °C	1.20	0.18
70 °C	1.10	0.18
60 °C	1.38	0.22
50 °C	1.66	0.23
30 °C	1.95	0.27

correlates with the higher hardness values in the hardness test.

Furthermore, the frictional force trend shown in Fig. 9b depicts a similar trend to that of the coefficient of friction in the temperature range studied. In explaining the tribological behavior of these coatings, two reasons are proposed for the varying behaviors, which are: First, the coatings deposited at bath temperatures of 70 °C and 80 °C have been observed to have the lowest roughness values, as indicated in the SEM and 3D topography profile results. This is suggestive of the fact that a reduction of the roughness of the

Cr coating by raising the bath temperature is the principal reason for the enhanced tribological behavior of the Cr coatings deposited at higher bath temperatures. Second, according to the study of others [37,38], the high COF value of coatings can be related to the micro-cracks extending throughout the coatings. Because of this, the lower wear resistance/higher COF of the Cr coatings deposited at 30 °C, followed by 50 °C and 60 °C is also attributed to the cracks observed on their surfaces.

In addition, in all bath temperature conditions, it is observed that during the initial ramping of the scratch test (i.e within the first 1 mm distance), the friction fluctuated drastically. This is a result of the interaction of the coatings and the ball materials [37,39]. The high initial COF value for all conditions was due to the adhesion wear that occurred between the coated samples and the ball. Also, it is important to point out that the coefficient of friction values obtained in this study showed values lower than values obtained from Cr coatings by previous researchers [40–43], which invariably connotes better wear resistance. This signifies an improved adhesion of the electrodeposited Cr coating to the SS substrate, and this improvement could be attributed to the new pretreatment method (anodic activation) developed in this study. The anodic activation method enabled a better removal of the quickly formed oxide film on the SS specimens, thereby allowing better deposition/adherence on the SS (as shown in the Supplementary Fig. S1), which increases the cathodic current efficiency of the electrodeposition process. The SEM images of the scratched Cr coated surfaces are presented in Supplementary Fig. S3.

3.4. Electrochemical behavior of the electrodeposited Cr coating

The electrochemical behavior of the electrodeposited Cr coating and the bare 304L SSs is investigated in 3.5 wt% NaCl environment with a potentiodynamic polarization test (performed only in the anodic branch), and the results are presented in the polarization curves in Fig. 10. As summarized in Table 5, the results reveal that the pitting potential of the Cr-coated samples are more positive than that of the bare 304L SS in the chloride-containing environment. This indicates that the Cr-coated 304L SS samples improved in pitting resistance, as compared to the uncoated SS base metal in 3.5 wt% NaCl environment. The improvement was more obvious for Cr-coated samples electrodeposited at bath temperatures of 70 °C and 80 °C, which are over 200 mV better in pitting resistance than the bare 304L SS base metal (as seen in Fig. 10).

Interestingly, it is noticed that the pitting current for the different conditions is quite complicated. In the cases of the electrodeposited Cr coatings at 30 °C (2.7×10^{-3} A) and 50 °C (6.6×10^{-4} A), the pitting currents were higher than that of the uncoated SS base metal (2.5×10^{-4} A). However, it was different in the Cr coatings deposited at 60 °C (1.7×10^{-4} A), 70 °C (1.6×10^{-5} A), and 80 °C (1.4×10^{-5} A), which showed lower pitting currents signifying better protection than the coating produced at bath temperatures of 30 °C and 50 °C. The reason for this behavior is a result of the high density of cracks experienced in the coatings produced at 30 °C and 50 °C bath temperature conditions, and the weaker adhesion of these coatings, as compared to those coatings produced at bath temperatures of 70 °C and 80 °C. To quantify the protection degree of the various electrodeposited Cr coatings to pitting corrosion, a formula deduced in previous study [44] was used, as shown in equation (4):

$$Z = \frac{E_{pit\ (Cr)} - E_{pit(SS)}}{E_{pit(Cr)}} \times 100\% \quad (4)$$

where $E_{pit(Cr)}$ and $E_{pit(SS)}$ are the pitting potentials of the Cr-coated 304L SSs and uncoated 304L SS base metal, respectively.

Using equation (4) and the electrochemical parameters of the coated and uncoated SSs summarized in Table 5, it is estimated that the degree of protection of the electrodeposited Cr coatings to pitting are in the following increasing order, 60 °C (69 %) < 50 °C (76 %) < 30 °C (89 %) < 70 °C (91 %) < 80 °C (93 %). This validates and quantifies the potentiodynamic polarization results, which shows that the almost crack-free Cr coatings deposited at higher temperatures are better resistant to pitting corrosion attacks in the chloride-containing environment used in this study. Interestingly, Cr coating deposited at 30 °C gave a better degree of protection to pitting than those deposited at 50 °C and 60 °C from the estimation despite its higher crack density. This estimation trend for the Cr coatings deposited at the studied bath temperatures agree with the passivation region duration trend shown in Table 5. The reason for this behavior may be due to the greater thickness of the Cr coating produced at 30 °C.

To further substantiate that the almost crack-free Cr coating deposited at bath temperatures of 70 °C and 80 °C gave better protection against pitting corrosion, SEM observation of the Cr coatings exposed to the 3.5 wt% NaCl solution (via potentiodynamic polarization tests) was carried out, and the results are presented in Fig. 11a(i)-f(i) and magnified images in Fig. 11a(ii)-f(ii). This study finding (in which almost crack-free coatings showed better pitting corrosion resistance) is in agreement with previous results of Chien C.W. et al. [17] and Ghaziof S. et al. [45] and others [46–48], who reported that coating defect like crack is detrimental to the integrity of coatings and should be eliminated as much as possible for an effective application.

Further analysis was carried out with a 3D profilometer to quantify the pitting corrosion degree on the surfaces of the Cr-coated 304L SSs and uncoated 304L SS base metal exposed to a chloride-containing environment (via potentiodynamic polarization examination). The results are depicted in Fig. 12a. To obtain deeper insight into the protection degree of the Cr coatings, the 3D topography maps were analyzed with Gaussian multimodal histogram and PSD analysis, as presented in Figs. 12b and 13a, respectively. The topography maps in Fig. 12a clearly represent the presence of intensive localized corrosion attacks including pitting corrosion and breakdown of polyhedral granules (due to high overpotential and its stress plus passive film breakdown) in bare 304L SS and Cr-coated surfaces electrodeposited at 30 °C and 50 °C. However, these localized corrosion attacks are reduced by increasing the temperature of the Cr electrodeposition bath to 60 °C (very fine pitting), 70 °C, and 80 °C (lowest pitting attacks and smooth surface). From the histogram analysis in Fig. 12b and its extracted results in Fig. 12c, it can be observed that the Cr-coated surface electrodeposited at high bath temperatures including 60 °C, and especially 70 °C, and 80 °C represent the lowest mean value of surface roughness distribution

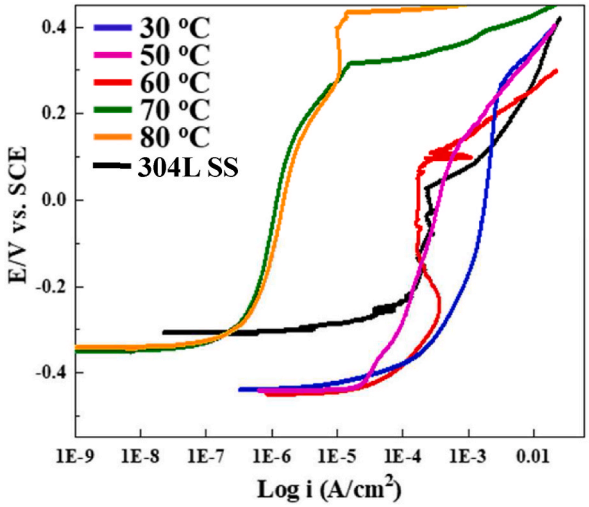

Fig. 10. Potentiodynamic polarization plots of uncoated 304L SS and Cr-coated 304L SS samples deposited at different bath temperatures (3.5 wt % NaCl solution).

Table 5
Electrochemical parameters were extracted from the potentiodynamic polarization curves of the bare 304L SS and the Cr coatings deposited at different bath temperatures.

Specimens	Open circuit potential (mV)	Pitting potential (E_{pit}, mV)	Pitting current (I_{pit}, A)	Passivation potential (E_{pass}, mV)	Passivation region duration (E_{pit} - E_{pass}, mV)
304L SS	−309.7	28.7	2.5×10^{-4}	−218.4	246.3
Cr coating (30 °C)	−437.2	272.6	2.7×10^{-3}	−293.1	563.9
Cr coating (50 °C)	−440.6	120.6	6.6×10^{-4}	−398.9	519.5
Cr coating (60 °C)	−447.2	93.3	1.7×10^{-4}	−259.6	352.9
Cr coating (70 °C)	−349.1	321.4	1.6×10^{-5}	−261.1	581.5
Cr coating (80 °C)	−340.8	436.2	1.4×10^{-5}	−266.4	702.2

and standard deviation value than those electrodeposited at low bath temperatures (30 °C and 50 °C).

To gain a profound insight into a visualization of various surface features and their distribution such as pitting corrosion regions, PSD analysis of all electrodeposited Cr coating after post-corrosion was conducted. In the PSD curves (Fig. 13), the highest and the lowest spatial frequencies are assigned to the deepest (pits and/or holes in cases of 304L SS, 30 °C, 50 °C, and 60 °C) and topmost surface features, respectively. By comparing the PSD profiles of all Cr-coated surfaces and bare 304L SS, an extra or higher PSD distribution can be detected at the high-frequency side of the PSD profiles between 1.5 and 6.2×10^6 m^{-1} only for Cr-coated surfaces electrodeposited at 30 °C, 50 °C, and 60 °C plus bare 304L SS. This occurrence is related to the presence of pitting corrosion attacks with the lowest height (the deepest pit as a hole shows the highest spatial frequency (Fig. 13b)). However, at the spatial frequency values between 5.8×10^5 to 1.5×10^6 m^{-1}, the lowest PSD magnitude can be observed only in Cr-coated surfaces electrodeposited at 70 °C and 80 °C. This further can confirm the presence of very small surface features with the lowest roughness distribution such as very fine corroded sites, similar to the result in Fig. 11.

Overall, the PSD roughness magnitude of Cr-coated surfaces electrodeposited at 70 °C and 80 °C in all spatial frequencies is lower than those of Cr coatings at 30 °C, 50 °C, and 60 °C, thus, further confirming the high corrosion protection behavior of Cr coatings (smooth surface confirms less pitting corrosion attacks) that are electrodeposited at high temperatures.

4. Conclusions

A direct current electrodeposition method was employed to prepare Cr coatings on the surface of 304L SS from a trivalent Cr-bath at different bath temperatures. The microstructure, surface topography, mechanical, and electrochemical behavior of these Cr-coated samples are investigated and the key findings are summarized as follows:

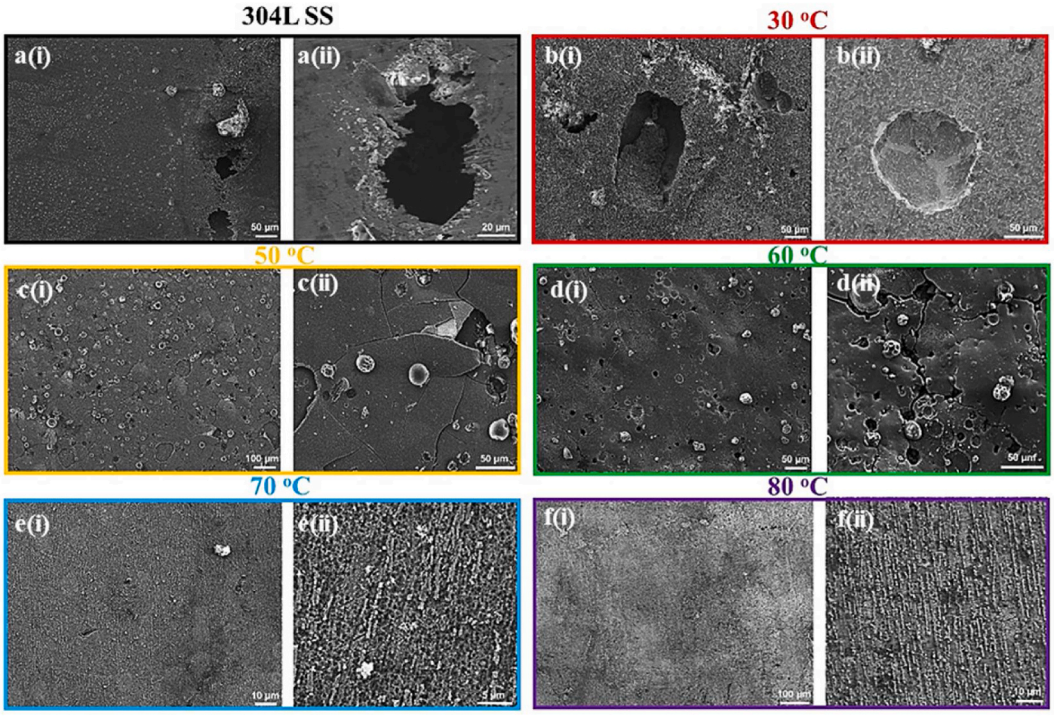

Fig. 11. SEM images of 304 L SS and Cr-coated 304L SSs after potentiodynamic polarization test in 3.5 wt% NaCl solution with low (a(i)-f(i)) and high magnification images (a(ii)-f(ii)).

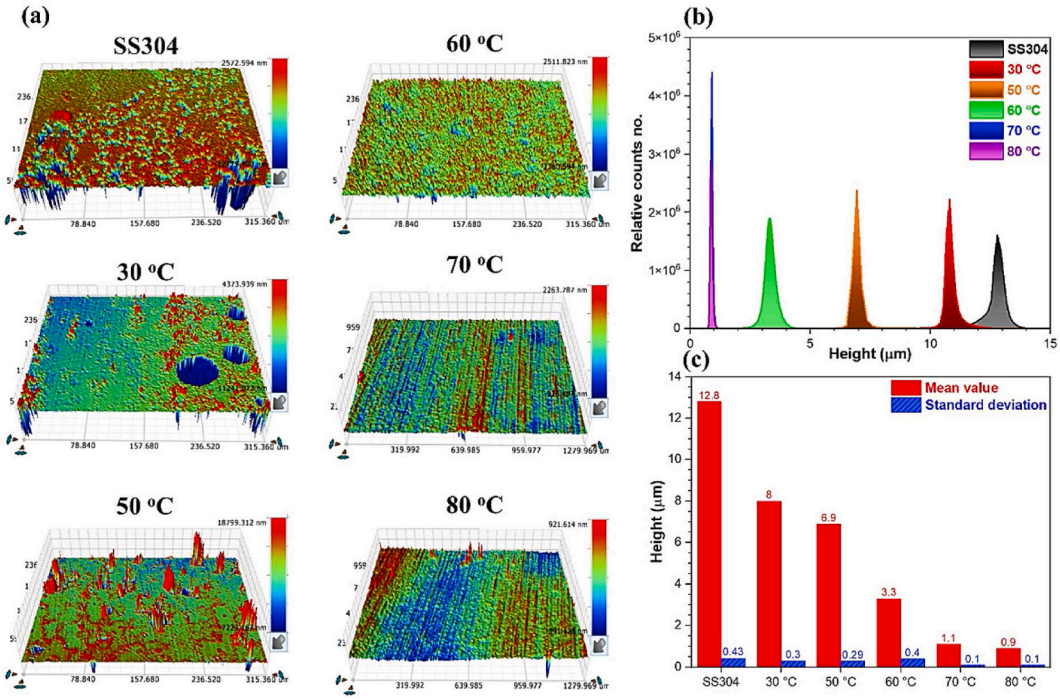

Fig. 12. (a) 3D topography profile maps of various Cr-coated 304L SS samples after potentiodynamic polarization in 3.5%wt. NaCl solution, (b) The multimodal Gaussian histograms of surface topography for various Cr-electrodeposited surfaces after potentiodynamic polarization in 3.5%wt. NaCl solution, (c) The extracted mean value and standard deviations of histogram curves in (b).

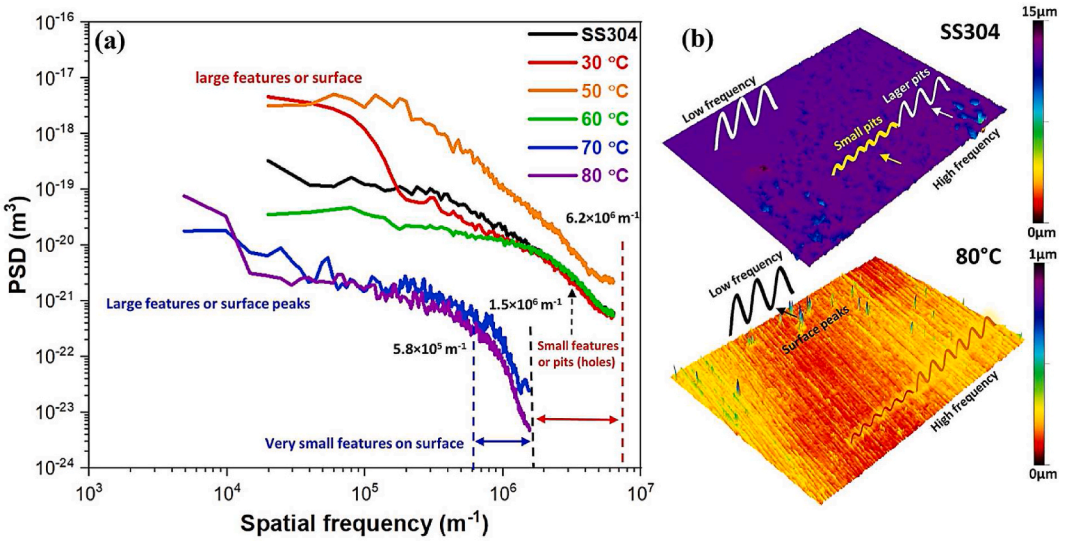

Fig. 13. (a) Power spectral density (PSD) analysis of surface topography for various Cr-electrodeposited surfaces after exposure to a corrosive environment, (b) A 3D topography representation of SS304 and Cr-electrodeposited coating (80 °C) alongside a correlation between the surface topography distribution and spatial frequency for various surface features.

1) The Cr deposits at all bath temperatures except for 80 °C showed clusters of polyhedral grains, however, the grain sizes decreased with higher bath temperatures. The presence of Cr, C, and S elements were observed in the Cr deposits, however, the presence of C and S varied with temperature change.
2) The SEM and 3D topography profile results indicated that increasing the electrolyte bath temperature leads to surface modification, with coatings deposited at higher temperatures showing smoother surfaces.
3) XRD analysis revealed that the Cr coating amorphization increases with a decline in electrolyte bath temperature, as evidenced by the broadening of the standard Cr peak at 44° for the Cr (110) plane. This increase is attributed to the increased in-corporation of the metalloid carbon atom.
4) The mechanical behavior of the various coatings showed that the hardness decreases as the bath temperature increases. Although, the Cr-coatings produced in this study showed overall good coating adhesion to the substrate, it was observed that the coating adhesion and wear resistance increased as bath temperature increased, with Cr coating deposited at 70 °C having the best tribological property.
5) The electrochemical results showed that the pitting potential of the Cr-coated samples at all bath temperatures were more positive than the pitting potential of the bare 304L SS in the chloride-containing environment used. Notwithstanding, it is important to point out that the improvement was more conspicuous for Cr-coated samples electrodeposited at bath temperatures of 70 °C and 80 °C.

Data availability

The organized data are available upon request to the corresponding author.

CRediT authorship contribution statement

Bright O. Okonkwo: Writing – original draft, Investigation, Formal analysis, Data curation, Conceptualization. **Chaewon Jeong:** Investigation, Formal analysis, Data curation. **Hyeon Bae Lee:** Formal analysis, Data curation. **Changheui Jang:** Writing – review & editing, Supervision, Conceptualization. **Ehsan Rahimi:** Formal analysis, Data curation. **Ali Davoodi:** Formal analysis, Data curation.

Declaration of competing interest

The authors declare that they have no known competing financial interests or personal relationships that could have appeared to influence the work reported in this paper.

Acknowledgements

This work is supported by the Nuclear R & D Program (No. 2019M2D2A2050927) of MSIT/NRF of the Republic of Korea. The helps from the KAIST Analysis Center for Research Advancement and Professor Sung Oh Cho laboratory at KAIST are acknowledged.

Appendix A. Supplementary data

Supplementary data to this article can be found online at https://doi.org/10.1016/j.heliyon.2023.e22538.

References

[1] S. Yeo, J.H. Kim, H.S. Yun, Effect of pulse current and coating thickness on the microstructure and FCCI resistance of electroplated chromium on HT9 steel cladding, Surf. Coat. Technol. 389 (2020), 125652.
[2] S. Yeo, J.H. Kim, S.H. Eom, The characterization of electrodeposited chromium barriers for nuclear reactor cladding application, J. Nucl. Mater. 530 (2020), 151980.
[3] B.O. Okonkwo, C. Jeong, C. Jang, Advances on Cr and Ni electrodeposition for industrial applications—a Review, Coatings 12 (2022) 1555.
[4] E. Beltowska-Lehman, P. Indyka, A. Bigos, M.J. Szczerba, J. Guspiel, H. Koscielny, et al., Effect of current density on properties of Ni–W nanocomposite coatings reinforced with zirconia particles, Mater. Chem. Phys. 173 (2016) 524–533.
[5] G. Barati Darband, M. Aliofkhazraei, S. Khorsand, S. Sokhanvar, A. Kaboli, Science and engineering of superhydrophobic surfaces: review of corrosion resistance, chemical and mechanical stability, Arab. J. Chem. 13 (2020) 1763–1802.
[6] P. Leisner, I. Belov, Influence of process parameters on crack formation in direct current and pulse reversal plated hard chromium, Trans. Inst. Met. Finish. 87 (2013) 90–96.
[7] Z.A. Hamid, M.A. Abbas, N. Gomaa, Enhancement of the properties of austenitic stainless steel by nickel diffusion coatings, Anti-Corros, Methods and Mater 50 (2003) 115–120.
[8] C.H. Hsu, T.C. Chen, R.T. Huang, L.W. Tsay, Stress corrosion cracking susceptibility of 304L substrate and 308L weld metal exposed to a salt spray, Mater 10 (2017) 1–14.
[9] H. Khani, J.F. Brennecke, Hard chromium composite electroplating on high-strength stainless steel from a Cr(III)-ionic liquid solution, Electrochem. Comm. 107 (2019), 106537.
[10] Z. Zeng, A. Liang, J. Zhang, A review of recent patents on trivalent chromium plating, Recent Pat. Mater. Sci. 2 (2009) 50–57.
[11] J.M. Olivares-Ramírez, M.L. Campos-Cornelio, J. Uribe Godínez, E. Borja-Arco, R.H. Castellanos, Studies on the hydrogen evolution reaction on different stainless steels, Int. J. Hydrog. Energy 32 (2007) 3170–3173.
[12] A. Elmeligi, N. Ismail, Hydrogen evolution reaction of low carbon steel electrode in hydrochloric acid as a source for hydrogen production, Int. J. Hydrog. Energy 34 (2009) 91–97.
[13] R.N. Gay, E. Palmer, W.K. Raymond, Process for Electroplating Nickel over Stianless Steel, United States Patent, 1988. No.4764260.
[14] R.A. Trammel, Method to improve the corrosion performance of microporous nickel deposit, Plat. Surf. Finish. 42 (1996) 24–28.
[15] B.O. Okonkwo, H. Ming, J. Wang, E.-H. Han, E. Rahimi, A. Davoodi, et al., A new method to determine the synergistic effects of area ratio and microstructure on the galvanic corrosion of LAS A508/309 L/308 L SS dissimilar metals weld, J. Mater. Sci. Technol. 78 (2021) 38–50.
[16] B.O. Okonkwo, H. Ming, Z. Zhang, J. Wang, E. Rahimi, S. Hosseinpour, et al., Microscale investigation of the correlation between microstructure and galvanic corrosion of low alloy steel A508 and its welded 309/308L stainless steel overlayer, Corrosion Sci. 154 (2019) 49–60.
[17] C.W. Chien, C.L. Liu, F.J. Chen, K.H. Lin, C.S. Lin, Microstructure and properties of carbon–sulfur-containing chromium deposits electroplated in trivalent chromium baths with thiosalicylic acid, Electrochim. Acta 72 (2012) 74–80.
[18] S. Mahdavi, S.R. Allahkaram, A. Heidarzadeh, Characteristics and properties of Cr coatings electrodeposited from Cr(III) baths, Mater. Res. Express 6 (2019), 026403.
[19] L. Philippe, C. Heiss, J. Michler, Electroplating of stainless steel, Chem. Mater. 20 (2008) 3377–3384.
[20] G. Ottewill, F. Walsh, The speed of metal deposition and dissolution, Trans. Inst. Met. Finish. 77 (1999) 209–211.
[21] M. Aliofkhazraei, F.C. Walsh, G. Zangari, H. Köçkar, M. Alper, C. Rizal, et al., Development of electrodeposited multilayer coatings: a review of fabrication, microstructure, properties and applications, Appl. Surf. Sci. Advances 6 (2021), 100141.
[22] Z. Zeng, L. Wang, A. Liang, J. Zhang, Tribological and electrochemical behavior of thick Cr–C alloy coatings electrodeposited in trivalent chromium bath as an alternative to conventional Cr coatings, Electrochim. Acta 52 (2006) 1366–1373.
[23] F.I. Danilov, V.S. Protsenko, V.O. Gordiienko, S.C. Kwon, J.Y. Lee, M. Kim, Nanocrystalline hard chromium electrodeposition from trivalent chromium bath containing carbamide and formic acid: structure, composition, electrochemical corrosion behavior, hardness and wear characteristics of deposits, Appl. Surf. Sci. 257 (2011) 8048–8053.
[24] C.A. Huang, Y.W. Liu, C. Yu, C.-C. Yang, Role of carbon in the chromium deposit electroplated from a trivalent chromium-based bath, Surf. Coat. Technol. 205 (2011) 3461–346246 6.
[25] National Institute of Standard Technology (NIST) Standard Reference Database 69: NIST Chemistry WebBook, 2022, https://doi.org/10.18434/T4D303 updated version.
[26] M.W. Chase, NIST-JANAF thermochemical tables reference data, Monograph 9, Fourth Edition, J. Phys. Chem (1998) 1–1951.
[27] Y. Wang, W. Zhou, Q. Wen, X. Ruan, F. Luo, G. Bai, et al., Behavior of plasma sprayed Cr coatings and FeCrAl coatings on Zr fuel cladding under loss-of-coolant accident conditions, Surf. Coat. Technol. 344 (2018) 141–148.
[28] A. Michau, F. Maury, F. Schuster, R. Boichot, M. Pons, Evidence for a Cr metastable phase as a tracer in DLI-MOCVD chromium hard coatings useable in high temperature environment, Appl. Surf. Sci. 422 (2017) 198–206.
[29] S.M. Martinuzzi, L. Donati, W. Giurlani, F. Pizzetti, E. Galvanetto, N. Calisi, et al., A comparative Research on corrosion behavior of electroplated and magnetron sputtered chromium coatings, Coatings 12 (2022) 257.
[30] R. Guillon, O. Dalverny, B. Fori, C. Gazeau, J. Alexis, Mechanical behaviour of hard chromium deposited from a trivalent chromium bath, Coatings 12 (2022) 354.
[31] K. Jin, Y. Jia, Z. Zhao, W. Song, S. Wang, C. Guan, Synthesis of chromium carbide nano-powders by microwave heating and their composition and microstructure change under gamma ray irradiation, Molecules 24 (2019) 2–10.
[32] A. Bahari A. Anasari, Z. Rahmani, Low temperature synthesis of La_2O_3 and CrO_2 by Sol–gel process, J. Eng. Technol. Research 3 (2011) 203–208.
[33] X. Zhang, X. Zhong, P.B. Visscher, P.R. LeClair, A. Gupta, Structural and magnetic properties of epitaxial CrO_2 thin films grown on TiO2 (001) substrates, Appl. Phys. Letters 102 (2013), 162410.
[34] J. Wang, P. Che, J. Feng, M. Lu, J. Liu, J. Meng, A large low-field tunneling magnetoresistance of CrO_2 (CrO_2/Cr_2O_3) powder compact with two coercivities, J. Appl. Phys. 97 (2005), 073907.
[35] A.M.A. Mohamed, A.M. Abdullah, N.A. Younan, Corrosion behavior of superhydrophobic surfaces: a review, Arab. J. Chem. 8 (2015) 749–765.
[36] H. Rashtchi, K. Raeissi, M. Shamanian, Y. Acevedo Gomez, C. Lagergren, R. Wreland Lindstrom, V. Rajaei, Evaluation of Ni-Mo and Ni-Mo-P electroplated coatings on stainless steel for PEM fuel cells bipolar plates, Adv. Fuel Cells 16 (2016) 784–800.
[37] M.G. Hosseini, S. Ahmadiyeh, A. Rasooli, S. Khameneh-asl, Pulse plating of Ni-W-B coating and study of its corrosion and wear resistance, Metall. Mater. Trans. 50 (2019) 5510–5524.
[38] K.H. Lee, D. Chang, S.C. Kwon, Properties of electrodeposited nanocrystalline Ni–B alloy films, Electrochim. Acta 50 (2005) 4538–4543.
[39] A. Ruden-Muñoz, E. Restrepo-Para, F. Sequeda, CrN coatings deposited by magnetron sputtering: mechanical and tribological properties, Dyna 82 (2015) 147–155.

[40] S. Podgoric, B.J. Jones, R. Bulpett, J. Franks, G. Troisi, Structure and tribological performance of diamond-like carbon based coatings for aerospace component processing, e-J. Surf. Sci. Nanotechnol. 7 (2009) 459–464.
[41] X. Wang, R. Zhang, T. Zhou, X. Wei, P. Liaw, R. Feng, et al., Microstructural evolution in chroming coatings friction pairs under dry sliding test conditions, Adv. Tribol. 2018 (2018) 1–6.
[42] M.A. Mekicha, M.B. de Rooij, D.T.A. Matthews, C. Pelletier, L. Jacobs, D.J. Schipper, The effect of hard chrome plating on iron fines formation, Tribol. Int. 142 (2020), 106003.
[43] K. Bobzin, T. Brögelmann, C. Kalscheuer, M. Thiex, Self-lubricating triboactive (Cr,Al)N+Mo:S coatings for fluid-free applications, J. Mater. Sci. 56 (2021) 15040–15060.
[44] F.I. Danilov, V.S. Protsenko, T.E. Butyrina, E.A. Vasil'eva, A.S. Baskevich, Electroplating of chromium coatings from Cr(III)-based electrolytes containing water soluble polymer, Prot. Met. 42 (2006) 560–569.
[45] S. Ghaziof, M.A. Golozar, K. Raeissi, Characterization of as-deposited and annealed Cr–C alloy coatings produced from a trivalent chromium bath, J. Alloys Compd. 496 (2010) 164–168.
[46] R.S. Bath, P. Nagaraj, S. Priyadarshini, Zn–Ni compositionally modulated multilayered alloy coatings for improved corrosion resistance, Surf. Eng. 37 (2021) 7555–7763.
[47] R.S. Bath, K. Venkatakrishna, A.C. Hegde, Surface structure and electrochemical behavior of zinc-nickel anti-corrosive coating, Anal. Bioanal. Electrochem. 15 (2023) 90–101.
[48] R.S. Bath, M.K. Balakrishna, P. Parthasarathy, A.C. Hegde, Structural properties of Zn-Fe alloy coatings and their corrosion resistance, Coatings 13 (2023) 772.